Journal of
Mechanical
Science and
Technology

Journal of Mechanical Science and Technology 21 (2007) 495~504

# Combustion Dynamics in a Model Lean-Premixed Gas Turbine with a Swirl Stabilized Injector

Hong-Gye Sung*

*School of Aerospace and Mechanical Engineering, Hankuk Aviation University*
*2001-1 Hwajeon-Dong, Deogyang-Gu, Goyang-City, Gyeonggi-Do, 412-791, Korea*

(Manuscript Received July 26 2006; Revised November 25, 2006; Accepted December 9, 2006)

**Abstract**

Unsteady numerical study has been conducted on combustion dynamics of a lean-premixed gas turbine with a swirl injector. A three-dimensional computation method utilizing large-eddy-simulation (LES) technique with finite rate chemical reaction was applied with the message passing interface (MPI) parallel architecture. The unsteady turbulent flame dynamics are carefully simulated so that the flow motion can be characterized in detail, showing fairly comparable results with the experimental data. It was observed that some fuel lumps escape from the primary combustion zone, and move downstream and consequently produce hot spots and large vortical structures in the azimuthal direction. The correlation between pressure oscillation and unsteady heat release is examined by the spatial Rayleigh parameter. In addition, it is shown that the complicate heat-release-structure can be precisely regenerated by means of modal analysis using proper orthogonal decomposition (POD).

*Keywords:* Combustion dynamics, Swirl combustion, LES, POD, Numerical analysis

## 1. Introduction

Gas turbines have traditionally used a diffusion-style combustor to supply reactants to the primary combustion region of the combustor. This produces a stable flame in the primary zone because combustion occurs at near stoichiometric conditions with reactants consumed at a rate controlled by the mixing of the fuel and air streams. Subsequent mixing with secondary and tertiary air streams reduces the gas temperature to the desired turbine inlet temperature. The diffusion combustor has another advantage in that fuel and air are mixed inside the combustor, thereby preventing flashback. But tighter regulation of $NO_x$ emissions favors the use of lean premixed (LPM) combustion. By premixing fuel and air upstream of the reaction region, LPM combustors avoid locally stoichiometric combustion, thus eliminates the high temperatures which may produce thermal $NO_x$.

Recently it was reported that oscillating combustion has emerged as a common problem in LPM combustor design. Oscillations occur when variations in heat release periodically couple to acoustic modes in a combustion chamber, producing significant pressure oscillations. These oscillations must be controlled because the resulting vibration can make the lifetime of engine shorten.

To resolve oscillation problems, it is helpful to understand the mechanisms that produce the variations in heat release and acoustic response. Oscillation in a combustor can be treated as a closed loop interaction between chemical reaction and acoustic wave generation (Richards 1996). A variation in heat release produces an acoustic disturbance that is reflected by the combustion walls, resulting in a pressure

*Corresponding author. Tel.: +82 2 300 0104; Fax.: +82 2 3158 4429
E-mail address: hgsung@hau.ac.kr

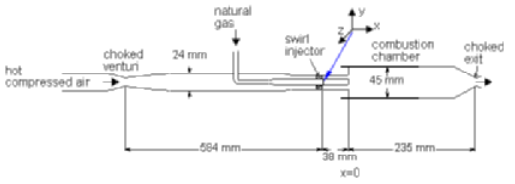


Fig. 1. Schematic of a model gas turbine combustor (Seo, 1999).

disturbance. The magnitude of the pressure disturbance is reduced by acoustic losses, but can otherwise pro-duce changes in the combustion process, thereby alerting heat release. For example, a momentary increase in combustor pressure will briefly reduce the airflow entering via the fuel nozzle. At a constant fuel flow, the reduced air flow will produce a slightly richer mixture, accelerating com-bustion. Thus, the pressure feedback has produced a variation in heat release which restarts the closed-loop cycle. With the correct timing of the feedback, and sufficiently small losses, the oscillation magnitude can grow to a limit cycle oscillation.

Most LPM systems stabilize the flame with recirculation developed by swirling flow. In case of unstable burning, Huang *et al.* (2003) emphasized that the energy release in the flame zone was fluctuated and derived acoustic waves in the combustor, using LES with flamelet model. Thus, the purposes of this study are to observe dynamic flow and unsteady heat release structure, and to understand the basic mechanism of closed-loop cycle between pressure oscillation and heat release by means of 3D dynamic compressible LES with finite-rate global-chemical reaction model. In addition, it was shown that the complicate heat release structure can be precisely generated from the base modal structures by proper orthogonal decomposition (POD). For this study, Seo's model combustor (Seo, 1999) with swirl stabilization was chosen as physical model (Fig. 1), which was conducted to understand the coupling mechanism between pressure oscillation and heat release, supported by GEAGTR(General Electric Advanced Gas Turbine Research) program.

## 2. Theoretical formulation

### *2.1 Governing equations*

The Favre averaged governing equations based on the conservation of mass, momentum, energy, and species concentration for a compressible, chemically reacting gas can be expressed as:

$$\frac{\partial \bar{\rho}}{\partial t}+\frac{\partial \overline{\rho u}_j}{\partial x_j}=0 \tag{1}$$

$$\frac{\partial \overline{\rho u}_i}{\partial t}+\frac{\partial(\overline{\rho u}_i\tilde{u}_j+\bar{p}\delta_{ij})}{\partial x_j}=\frac{\partial\left(\bar{\tau}_{ij}-\tau_{ij}^{sgs}\right)}{\partial x_j} \tag{2}$$

$$\frac{\partial \overline{\rho E}}{\partial t}+\frac{\partial((\overline{\rho E}+\bar{p})\tilde{u}_i)}{\partial x_i}=\frac{\partial}{\partial x_i}\left(\tilde{u}_j\bar{\tau}_{ij}+\kappa\frac{\partial \bar{T}}{\partial x_i}-H_i^{sgs}+\sigma_i^{sgs}\right) \tag{3}$$

$$\frac{\partial \overline{\rho Y}_k}{\partial t}+\frac{\partial\left(\overline{\rho u}_j\tilde{Y}_k\right)}{\partial x_j}=\frac{\partial}{\partial x_j}\left(\overline{\rho U}_{k,j}\tilde{Y}_k-\Phi_{k,j}^{sgs}-\theta_{k,j}^{sgs}\right)+\overline{\dot{\omega}}_k \tag{4}$$

The subgrid closure terms are given by:

$$\tau_{ij}^{sgs}=\bar{\rho}\left(\widetilde{u_iu_j}-\tilde{u}_i\tilde{u}_j\right) \tag{5}$$

$$H_i^{sgs}=\bar{\rho}\left(\widetilde{Eu}_i-\tilde{E}\tilde{u}_i\right)+\left(\widetilde{pu}_i-\bar{p}\tilde{u}_i\right) \tag{6}$$

$$\sigma_{ij}^{sgs}=\left(\widetilde{u_j\tau_{ij}}-\tilde{u}_j\bar{\tau}_{ij}\right) \tag{7}$$

$$\Phi_{k,j}^{sgs}=\bar{\rho}\left(\widetilde{Y_ku_j}-\tilde{Y}_k\tilde{u}_j\right) \tag{8}$$

$$\Theta_{k,j}^{sgs}=\bar{\rho}\left(\widetilde{Y_kU_{k,j}}-\tilde{Y}_k\tilde{U}_{k,j}\right) \tag{9}$$

The terms $\tau_{ij}^{sgs}$, $H_i^{sgs}$, and $\phi_{\mathrm{k,j}}^{\mathrm{sgs}}$ result from filtering the convective terms. The other terms, $\sigma_{ij}^{sgs}$ and $\Theta_{k,j}^{sgs}$, come from correlations of the velocity field with the viscous stress tensor, and the species mass fractions with the diffusion velocities, respectively. The more detail formulations with global finite rate reaction mechanism of Methane ($CH_4$) are addressed in the reference (Sung, 1999).

### *2.2 Subgrid Scale turbulence model*

The compressible version of the dynamic Smagorinsky model (DSM) is employed in the present study. The assumption of the algebraic Smagorinsky-type model is the equilibrium flow of turbulent energy cascade, and model coefficients are determined from isotopic turbulence decay. Moreover, the model coefficients are prescribed *a priori* and remain a constant, which implies their inability to model correctly the unresolved subgrid stresses in different type of

turbulent flow fields. The introduction of dynamic models circumvents this basic assumption in order to compute non-equilibrium flow by calculating the model coefficients directly (i.e., as a function of space and time during the simulation) thus providing the proper local amount of subgrid mixing and dissipation. Another important idea in SGS modeling involves scale similarity, which assumes that the largest of the unresolved scales, which contain most of the SGS energy, have a similar structure to the smallest of the resolved scales (Germano *et al.*, 1991). The various dynamic models have been shown the possibility of the application of LES to a variety flow of complex engineering geometry (Moin, 1997 ).

To employ the basic idea of scale similarity (i.e., the largest of the unresolved scales have a similar structure to the smallest of the resolved scales), two filtering operators are defined: one is the grid filter, $G$ while the other is the test filter, $\hat{G}$ or $< G >$ as:

$$\overline{\phi}(x) = \int_{-\infty}^{\infty} G(x-\xi)\ \phi(\xi)\ d\xi \tag{10}$$

$$\hat{\phi}(x) = \langle \phi \rangle = \int_{-\infty}^{\infty} \hat{G}(x-\xi)\ \phi(\xi)\ d\xi \tag{11}$$

The filter width of the test filter is assumed to be larger than that of the grid filter. It is noted that two times of the filter width of the grid filter ( $\overline{\Delta}$ ) is assigned to that of the test filter ( $\hat{\Delta}$ ) in the present study, (i.e., $\hat{\Delta} = 2\overline{\Delta}$ for one direction).

Both subgrid stress $\tau_{ij}^{sgs}$ and subtest stress $T_{ij}$ can be modeled in the same way as the compressible Smagorinsky model:

$$\tau_{ij}^{sgs} - \frac{\delta_{ij}}{3}\tau_{kk}^{sgs} = -2C_R\overline{\Delta}^2\overline{\rho}\left|\widetilde{S}\right|\left(\widetilde{S}_{ij} - \frac{\delta_{ij}}{3}\widetilde{S}_{ll}\right) = C_R\alpha_{ij} \tag{12}$$

$$T_{ij} - \frac{\delta_{ij}}{3}T_{kk} = -2C_R\hat{\Delta}^2\hat{\overline{\rho}}\left|\widetilde{\widetilde{S}}\right|\left(\widetilde{\widetilde{S}}_{ij} - \frac{\delta_{ij}}{3}\widetilde{\widetilde{S}}_{ll}\right) = C_R\beta_{ij} \tag{13}$$

where

$$\alpha_{ij} = -2\overline{\Delta}^2\overline{\rho}\left|\widetilde{S}\right|\left(\widetilde{S}_{ij} - \frac{\delta_{ij}}{3}\widetilde{S}_{ll}\right)$$

$$\beta_{ij} = -2\hat{\Delta}^2\hat{\overline{\rho}}\left|\widetilde{\widetilde{S}}\right|\left(\widetilde{\widetilde{S}}_{ij} - \frac{\delta_{ij}}{3}\widetilde{\widetilde{S}}_{ll}\right) \tag{14}$$

Then, the anisotropic ($C_R$) and isotropic ($C_I$) model coefficients of SGS stress are obtained as:

$$C_R = \frac{L_{u_iu_j}M_{u_iu_j}}{M_{u_ku_l}M_{u_ku_l}}\ C_I = \frac{L_{u_ku_k}}{\beta - \hat{\alpha}} \tag{15}$$

The resolved turbulent stress, $L_{ij}$, are representative of the contribution to the Reynolds stresses by the scales whose lengths are intermediate between the grid filter width and the test filter width as follows:

$$L_{u_iu_j} = \left\langle \overline{\rho}\widetilde{u}_i\widetilde{u}_j \right\rangle - \frac{\left\langle \overline{\rho}\widetilde{u}_i \right\rangle\left\langle \overline{\rho}\widetilde{u}_j \right\rangle}{\left\langle \overline{\rho} \right\rangle} \tag{16}$$

The quantity $M_{u_iu_j}$ represents the differences between the model forms of the SGS stress tensor and subtest-stress tensor filtered at the test-filter level for the gradient diffusion as:

$$M_{u_iu_j} = \beta_{ij} - \hat{\alpha}_{ij} \tag{17}$$

The same idea of modeling SGS turbulent stress and SGS enthalpy are employed to dynamically calculate the turbulent Prandtl number in the SGS enthalpy flux model equation, which are described in the reference (Sung, 1999).

## 3. Numerical method

A three dimensional time-accurate scheme based on semi-implicit Runge-Kutta time marching scheme and finite volume in space integration is used in this present work.

One of the concerns in handling the chemical reacting term is the stiffness of the equations, since chemical processes have a wide range of time scales which are much smaller than the flow ones. As a result, if explicit methods are used to integrate the stiff governing equations, the computations will become inefficient, because the time step sizes directed by the stability requirements are much smaller than those required by the accuracy considerations. To overcome the stiffness problem, the additive semi-implicit method is introduced (Chiu *et al.*, 1996), which additively splits the governing equations into stiff and non-stiff terms. The stiff terms are treated implicitly, while the non-stiff ones are treated explicitly. To advance simultaneous high-order temporal accuracy and good stability properties, additive semi-implicit RK formulations have been developed by

Zhong (1996):

$$\left[I - \Delta t a_1 J(\hat{Q}^n)\right] q_1 = \Delta t\left\{f\left(\hat{Q}^n\right) + g\left(\hat{Q}^n\right)\right\} \quad (18)$$

$$\left[I - \Delta t a_2 J(\hat{Q}^n + c_{21} q_1)\right] q_2 = \Delta t\left\{f\left(\hat{Q}^n + b_{21} q_1\right) + g\left(\hat{Q}^n + c_{21} q_1\right)\right\} \quad (19)$$

$$\left[I - \Delta t a_3 J(\hat{Q}^n + c_{31} q_1 + c_{32} q_2)\right] q_3 = \Delta t\left\{f\left(\hat{Q}^n + b_{31} q_1 + b_{32} q_2\right) + g\left(\hat{Q}^n + c_{31} q_1 + c_{32} q_2\right)\right\} \quad (20)$$

$$\hat{Q}^{n+1} = \hat{Q}^n + \omega_1 q_1 + \omega_2 q_2 + \omega_3 q_3 \quad (21)$$

$q_1$, $q_2$, and $q_3$ are intermediate results. $g$ is the vector resulting from the spatial discretization of the stiff term (i.e., heat source), and $f$ is the vector resulting from the spatial discretization of the non-stiff terms (i.e., the rest of the terms except of heat source). The Jacobian matrix $J$ is based on only the stiff term $g$ (i.e., $J \equiv \partial g / \partial \hat{Q}$).

The explicit parameters are:

$\omega_1 = 1/8$, $\omega_2 = 1/8$, $\omega_3 = 3/4$

$b_{21} = 8/7$, $b_{31} = 71/252$, $b_{32} = 7/36$

and the implicit parameters are:

$a_1 = 0.797097$, $a_2 = 0.591381$, $a_3 = 0.134705$

$c_{21} = 1.05893$, $c_{31} = 1/2$, $c_{32} = -0.375939$

Further efficiency is obtained by implementing an MPI (Message Passing Interface) parallel computing architecture with a multi-block technique. To implement parallel computation, the computational domain is divided into 102 blocks and each block is assigned to each processor. Total 102 processors of Cray T3E are applied.

## 4. Computational condition

The model gas turbine combustor using NG (natural gas) consists of a single-swirl injector, a combustion chamber, and a nozzle as shown in Fig. 1 (Seo, 1999). The swirler has eight straight, flat vanes with a 45-degree swirl angle. The inside diameter of the combustion chamber is 45 mm with an aspect ratio, $A_{inlet}/A_c$, of 0.16 and a length of 207 mm. The nozzle with a 30-degree converging angle acoustically isolates the combustion chamber from its downstream conditions when it becomes chocked. The swirl number, S, based on swirler geometry can be defined as:

$$S = \frac{2}{3}\left[\frac{1-(D_h/D_n)^3}{1-(D_h/D_n)^2}\right]\tan\varphi \quad (22)$$

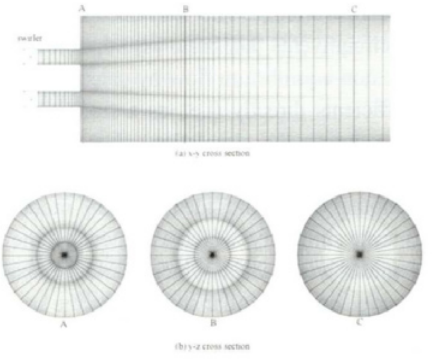


Fig. 2. Computational grid (135× 110 × 81).

where $D_h$, $D_n$, and $\varphi$ are the hub diameter, hub outer diameter, and swirl vane angle, respectively. The estimated swirl number is 0.69 for a 45-degree swirler.

The computational domain consists of a coaxial injector and a combustion chamber without a nozzle (Fig. 2). The three-dimensional grid was generated by rotating the two-dimensional grid with respect to the combustor centerline, and the grid had 135× 110 × 81. Of the 135 axial grid points, 25 points are used to cover the inlet section (upstream of the expansion). The axial and radial grids are non-uniform, (i.e., clustered at the shear layer and near the connection surface between the inlet and the combustor chamber), but the azimuthal grid is uniform. The basic scales of combustor in computational domain are the same as those in the experimental facilities, but the nozzle is not included to save the total number of grid points for economic computation. Thus, the boundary conditions should be carefully applied without contaminating the experiment's conditions. According to the experiment (Seo, 1999), this model combustor shows a dominant 1L mode with its harmonics, which implies a node point of acoustic wave at the middle of the chamber. Thus, it is notable that the computational chamber length is chosen to be half of the experimental chamber length, with the non reflecting boundary conditions (Poinsot *et al.*, 1992) of a constant back-pressure (4.05 atm.) on the exit surface. At the inlet boundary, the velocity components in the *x*-, *y*-, and *z*-directions, mass flow rate, and local temperature are specified. The x-directional velocity follows $1/7^{th}$ power based on the fully developed turbulent velocity profile, and azimuthal velocity is assumed to be proportional to the axial direction velocity (u=78 m/s) by a factor of the tangent of the swirl vane angle. The turbulent inlet boundary conditions are provided

by superimposing a time-dependent 5% fluctuation with Gaussian distribution onto a time-independent mean profile. The wall boundary conditions are assumed to be adiabatic. The time step is in the order of $0.2e^{-7}$ with 0.7 CFL (Courant-Friedrichs and Lewy) number.

In this study, the equivalence ratio 0.6 and inlet total temperature 670 K (assuming perfect premixed state) are chosen as the simulation conditions on that the limited unstable burning was observed in the experiment (Seo, 1999).

## 5. Results and discussion

### *5.1 Vortex breakdown*

Figure 3 represents the comparison of the Methane ($CH_4$) flame temperatures between the detailed chemical reaction mechanism using CEA (Gordon *et al.*, 1994) and the global reaction mechanism (Westbrook, 1981) used in this study to the fuel temperature ($T_{fi}$).

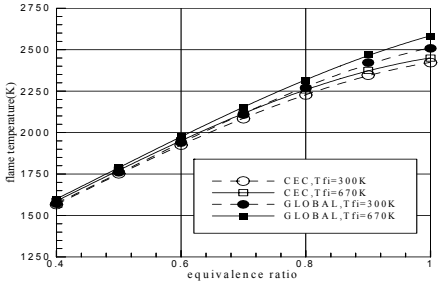


Fig. 3. The comparison of flame temperatures of $CH_4$ based on the detail chemical reacting mechanism and the global reacting mechanism.

Based on this baseline work, the flame temperature of the numerical computation of this study (2080 K) at equivalence ratio 0.6 is somewhat higher than the estimated temperature (1980 K), but still acceptable (see Fig. 5). Fig. 4 represents vorticity intensity on the x-y and y-z plane respectively. Many strong vortical motions are activated remarkably: especially at the shear layer near the dump plane, around the wrinkled flame surface, and at the vortex breakdown region caused by swirl directional velocity compo-nents. The strong vorticity leaving the dump plane of the combustor moves further downstream and dies out, while the vorticity caused by wrinkled flame survives as long as the life of local fuel lumps. Moreover, the vortices are processing downstream with accompanying irregular breaking strength, (i.e., vortex breakdown), and spiral into the core after vortex breakdown as well known as the proceeding process of vortex breakdown. In addition, Fig. 4e through 4g may infer the processing vortex core along near the centre line, pointed by previous researches (Lilley, 1977; Gupta *et al.*, 1984).

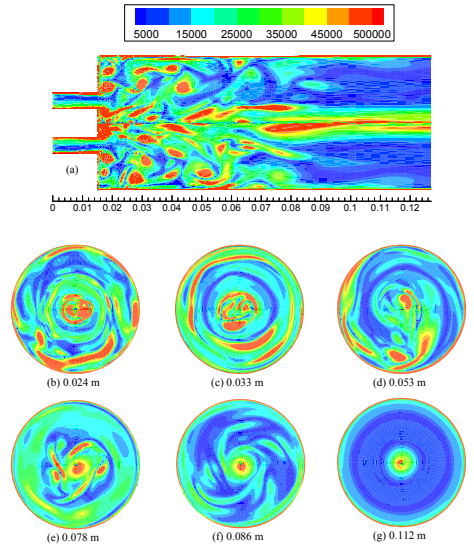


Fig. 4. Vorticity intensity structures on x-y and y-z cross sections at a typical time.

### *5.2 Coupling between oscillating pressure and fluctuating heat release*

Figure 5 shows the interaction between flow and

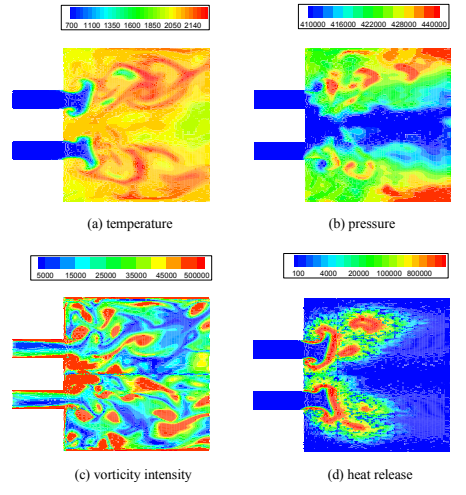


Fig. 5. The relations among temperature, pressure, voticity, and heat release at a typical time.

thermal structure, which closely interacts. The high temperature surrounds both main fuel stream and local fuel lumps. Some fuel lumps escape from the primary combustion zone, and consequently produce hot spots and large vortical structures in the azimuthal direction. In addition, the vortical structure induces pressure oscillation. Therefore, the flame environments become oscillatory, which may induce combustion instabilities.

Figure 6 compares the $CH_4$ heat release rate ($\dot{\omega}_{CH_4}\Delta H_f$) of the computational results and the CH* images of the experimental data. Flame size and shape compare well to each other, and almost chemical reactions take place near the dump plane of the combustion chamber. From both experiment data and computational results, it can be observed that fuel lumps are escaping from a primary combustion zone at $2\pi/3$, thus decreasing flame size. The flame also stretched after $\pi$. Those flame dynamics coincide with each other. In addition, Fig. 7 shows the volumetric release rate is dynamically changing in radial direction, bulging or shrinking at a certain phase, resulting three dimensional heat-release-structure.

The effect of heat release induced by chemical reaction on combustor stability characteristics can be investigated using Rayleigh's criterion (Rayleigh, 1945). The local Rayleigh index, $R(x)$, is defined as the mean value of the product of the pressure oscillation $p'(x,t)$ and heat release fluctuation $q'(x, t)$:

$$R(x) = \frac{1}{T}\int_T R(x,t)\,dt = \frac{1}{T}\int_T p'(x,t)q'(x,t)\,dt \qquad (23)$$

where $T$ is the time period of oscillation. The oscillation of pressure is amplified if $R(x) > 0$, while damped out and stabilized if $R(x) < 0$. Fig. 8 represents a Rayleigh index normalized by the maximum $R(x)$ in the x-y plan and the y-z plane. The major part, except a local area in the combustor, has positive Rayleigh parameters, indicating that pressure fluctuation and unsteady heat release are closely correlated (Fig. 8). The positive and negative Rayleigh

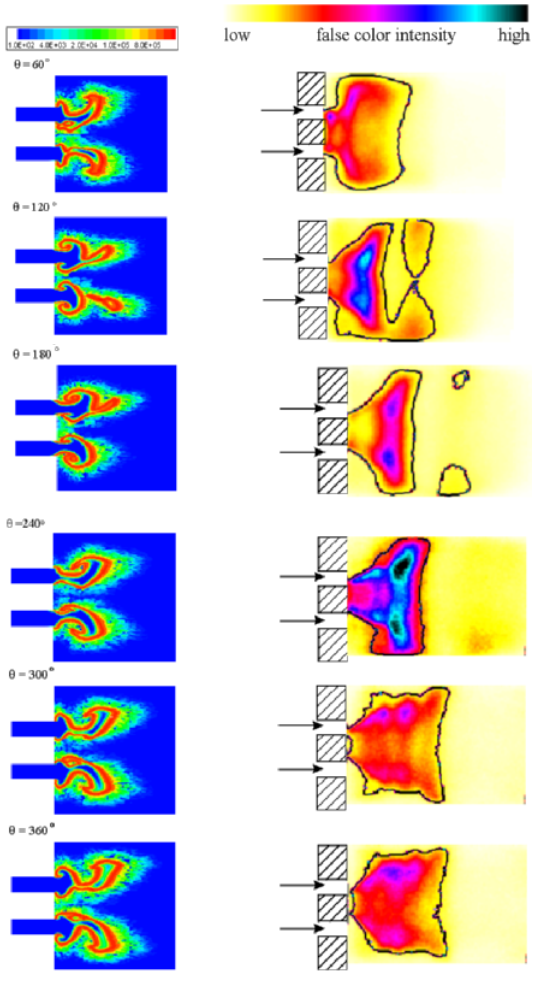


Fig. 6. Comparison of flame shape between computational results (a) and experimental results (b): (a) $CH_4$ heat release rate contours and (b) CH* emission image (Seo, 1999).

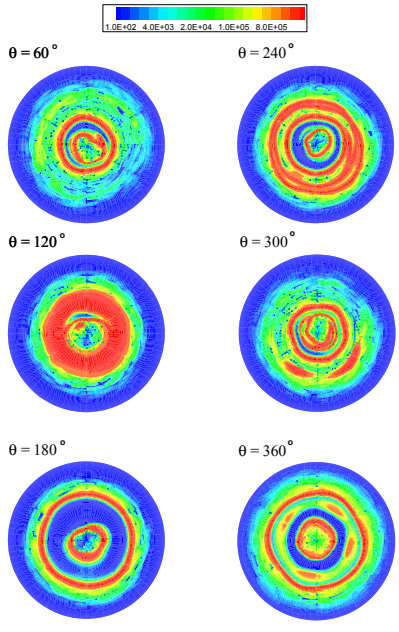


Fig. 7. Heat release rate near the primary combustion zone (x= 0.023 m) on the y-z plane over a typical cycle.

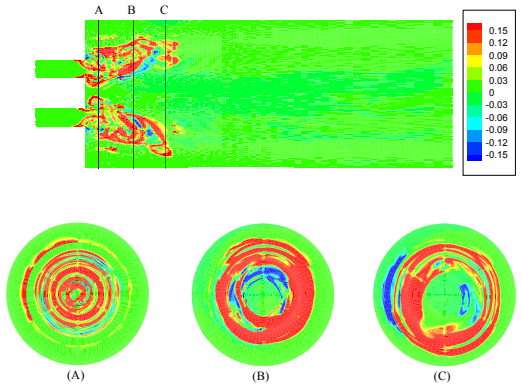


Fig. 8. Spatial Rayleigh parameters on the x-y and y-z planes.

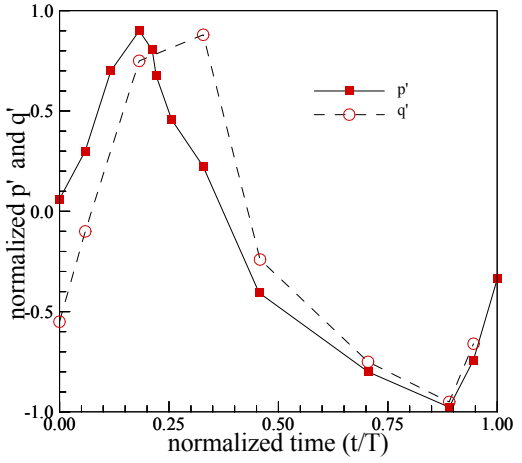


Fig. 9. Normalized pressure {p'} and heat release (q') fluctuation.

parameters can not be regionalized definitely but locally distributed, which is not recognized in previous research using flamelet model (Huang *et al*, 2003). The total heat flux in the combustion chamber fluctuates with less than one quarter lag to the chamber pressure as observed in the experiment (Fig. 9). This result tells that the pressure oscillations precede the heat release fluctuations, and the characteristic frequency will be lower than the resonant frequency. The RMS (root mean square) value of pressure fluctuation is about 0.4 atm.

### *5.3 Modal analysis*

As shown in previous sections, a turbulent flame in swirling environments is so complex that any analytical model may not diagnose swirling turbulent combustion properly — especially in confined geo-metry — even though the characterization of it is a milestone in current and future research work to actively control combustion instability. One of the primary motivations of this section is to identify those features of swirling turbulent flame structures based on the computational results of this study described in the previous section. To this end, modal signal processing of Proper Orthogonal Decomposition (POD) method (Sirovich, 1987; Sirovich *et al.*, 1992) is carried out. Physically, the POD has been applied with a considerable success to a wide variety of areas, ranging from free shear flows (Sirovich *et al.*, 1990) to flames (Torniainen *et al.*, 1997). The POD has also been applied to a turbulent channel flow, and a numerical validation of low-dimensional models based on the POD has already been established (Podvin *et al.*, 1998).

Table 1. Eigenvalues based on heat release.

| Number(*i*) | $\lambda_i$ | $\sum_{k=1}^{i}\lambda_k / \sum_{k=1}^{m}\lambda_k \times 100(\%)$ |
|---|---|---|
| 1 | 0.1936 | 19.3645 |
| 2 : | 0.1213 | 31.4937 |
| 3 : | 0.1120 | 42.6957 |
| 4 : | 0.0820 | 50.8987 |
| 5 : | 0.0782 | 58.7163 |
| 6 : | 0.0659 | 65.3059 |
| 7 : | 0.0573 | 71.0384 |
| 8 : | 0.0529 | 76.3295 |
| 9 : | 0.0417 | 80.5015 |
| 10 : | 0.0308 | 83.5862 |
| 11 : | 0.0277 | 86.3610 |
| 12 : | 0.0232 | 88.6849 |
| 13 : | 0.0204 | 90.7255 |
| 14 : | 0.0199 | 92.7174 |
| 15 : | 0.0189 | 94.6090 |
| 16 : | 0.0158 | 96.1851 |
| 17 : | 0.0142 | 97.6058 |
| 18 : | 0.0133 | 98.9396 |
| 19 : | 0.0106 | 100.0000 |
| 20 : | 0.0000 | 100.0000 |

A succinct general description of the POD is noted. If the heat release $q_i$ represents the deviation from the mean value $q_{mean}$ of snapshot $j$, we can construct the array of inner products:

$$\begin{bmatrix} (q_1,q_1) & (q_1,q_2) & \cdots & (q_1,q_m) \\ (q_2,q_1) & (q_2,q_2) & \cdots & (q_2,q_m) \\ \cdots & \cdots & \cdots & \cdots \\ (q_m,q_1) & (q_m,q_2) & \cdots & (q_m,q_m) \end{bmatrix} \tag{24}$$

and determine an optimal set of eigenmodes spanning the original set of snapshots using the eigen-vectors $e_i$ of Equation (24). Each element, $e_{j,i}$, contributes snapshot $j$ to eigenmode $i$, and the empirical eigenfunctions are computed by:

$$\psi_i(x) = \sum_j^m e_{j,i} q_j(x) \tag{25}$$

With each eigenmode, $\psi_i$ is associated with an eigenvalue of $\lambda_i$, which corresponds to the probability of finding that eigenfunction in the time-dependent flow field from which the snapshots were extracted:

$$\lambda_i = [(q_1, \psi_i)^2 + (q_2, \psi_i)^2 + \ldots + (q_m, \psi_i)^2] / m \tag{26}$$

Then, an optimal set of trial functions should capture as much energy as possible in as few modes as possible. These empirically determined eigen-modes can be used to decompose the snapshots of the dynamically changing flowfield and to quantify the growth rates of these modes. Meanwhile, we can also reverse the decomposition procedure and reconstruct the flow field from the basis modes and the empirical eigenfunctions.

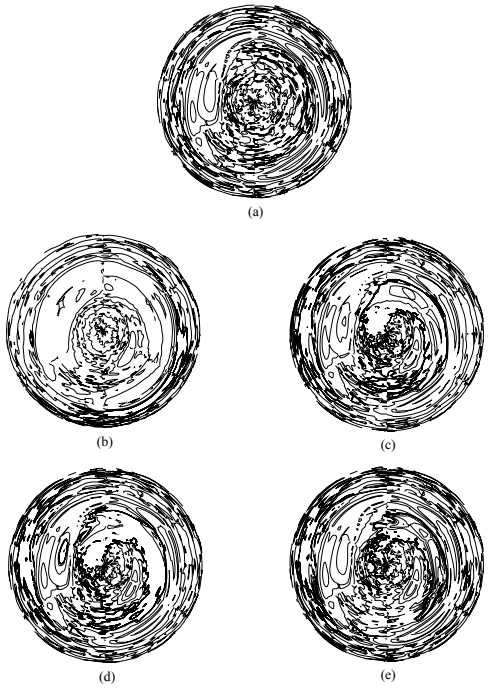


Fig. 10. Comparison of heat release between actual instantaneous contours (a) and reconstructed contours at x=0.023 m, using (b) first 3 basis modes; (c) first 6 basis modes; (d) first 9 basis modes; (e) first 12 basis modes. Solid lines denote positive values and dashed lines denote negative values. Contour levels shown are between 0 and 10e7.

POD was applied to characterize the basis eigenmode of heat release patterns in turbulent swirling combustion. First, we constructed the array of inner products based on the three-dimensional heat release data, then got an optimal set of trial functions with corresponding eigenvalues. Table 1 shows the eigenvalues with the associated energy corresponding to heat release, from which approximately 90 % of the energy is captured in the first thirteen modes. Fig. 10 shows the comparison of $CH_4$ heat release struc-tures between the actual instantaneous contours and the constructed contours using basis modes. The reconstruction data using the first twelve basic modes (Fig. 10e) provide comparable results, which imply the availability of the POD method. This information will be useful to anyone interested in active control of flame, since we can anticipate flame structure as well as generate an instantaneous flame structure very quickly and precisely at a typical moment we want to investigate.

## 6. Conclusions

The swirl-stabilized gas turbine engine was investigated using three-dimensional numerical analysis with an MPI parallel computing architecture. The conservation equations, including finite chemical reaction rate and dynamic large eddy simulation, were solved by finite volume numerical scheme in space and semi-implicit Runge-Kutta time marching technique.

A lean premixed combustor equivalence ratio 0.6 with high swirl rate (swirl number 0.69), was analyzed by eva-luating of a fluctuating flame behavior and unsteady heat release. The unsteady flame with burning on a double-side surface of a fuel stream is reduced as fuel lumps escape from the primary combustion zone at about 120 degrees (phase angle) of pressure fluctu-ation in the combustion chamber, and then growing/ stretching back to the original shape. This behavior corresponds to previous experiments governed domi-nantly by 1L mode of acoustic waves in combustor. In addition, it was observed that the escaped fuel lumps generate not

only a strong vorticity core at the moment of break from main fuel stream, but high heat spots inducing prompt thermal $NO_x$ formation. A more complex vorticity structure of chemical reacting flow than the cold flow case may disprove the close interaction between thermal structure and flow struc-ture, which are also visualized through a snapshot of temperature, pressure, vorticity, and heat release at a typical moment. The coupling between unsteady heat release and pressure fluctuation has lag less than one quarter. When performing a Rayleigh criterion analy-sis, the spatial Rayleigh parameter was positive. The complicate heat-release-structure can be precisely regenerated by the means of modal analysis using POD.

## Nomenclature

| | |
|---|---|
| $A$ | Area |
| $C_I$ | Isotropic model coefficient |
| $C_R$ | Anisotropic model coefficient |
| $D$ | Diameter |
| $e$ | Eigen vector |
| $E$ | Specific total energy |
| $G$ | Filter function |
| $H$ | Enthalpy |
| I | Identical matrix |
| $J$ | Jacobian matrix |
| $k$ | Heat conductivity or turbulent kinetic energy |
| $p$ | Pressure |
| $q$ | Heat release quantity |
| $Q$ | Conserved variable vector |
| $R$ | Rayleigh index |
| $S$ | Swirl number |
| $T$ | Temperature or time period of oscillation |
| $t$ | Time |
| $U_k$ | Diffusion velocity of species $k$ |
| $u$ | Velocity |
| $x$ | Spatial coordinate |
| $Y_k$ | Mass fraction of species $k$ |

## Greek symbols

| | |
|---|---|
| $\Delta$ | filter width or temporal width |
| $\delta$ | Chronicler delta |
| $\varphi$ | swirler vane angle |
| $\tau_{ij}$ | viscous stress tensor for a Newtonian fluid |
| $\theta$ | phase angle |
| $\rho$ | density |
| $\dot{\omega}$ | net production rate of chemical reaction |

## Subscripts

| | |
|---|---|
| $i$ | spatial coordinate index |
| $j$ | spatial coordinate index |
| $k$ | spatial coordinate index |
| $R$ | reference value |

## Superscripts

| | |
|---|---|
| $Sgs$ | subgrid scale |
| $\bar{}$ | time or space average |
| $\sim$ | Favre average |
| $\wedge$ | quantities associated with test filter |
| $'$ | fluctuation |

## References


Chiu, C. E., Zhong, X., 1996, "Numerical Simulation of Transient Hypersonic Flow Using the Essentially Nonoscillatory Schemes," *AIAA Journal*, Vol. 34, No. 4, pp. 655~661.

Huang, Y., Sung, H.-G., Hsieh, S. Y., Yang, V., 2003, "Large-Eddy Simulation of Combustion Dynamics in Lean-Premixed Swirl-Stabilized Combustors," *Journal of Propulsion and Power*, Vol. 19, No. 5, pp. 782~794.

Lilley, D. G., 1977, "Swirl Flows in Combustion: a Review," *AIAA Journal,* Vol.15, pp. 1063~1077.

Germano, M., Piomelli U., Moin, P., Cabot, W., 1991, "A Dynamic Subgrid-Scale Eddy Viscosity Model," *Phys. Fluid A*, Vol. 3(7).

Gordon, S., McBride, B. J., 1994, "Computer Program for Calculation of Complex Chemical Equilibrium Composition and Applications," NASA-RP-1311, Vol. I & II.

Gupta, A. K., Lilley, D. G., Syred, N., 1984, Swirl Flows, Abacus Press.

Moin, P., 1997, "Progress in Large Eddy Simulation of Turbulent Flows," AIAA 97-0368.

Podvin, B., Lumley, J. L., 1998, "A Low-Dimensional Approach for the Minimal Flow Unit," *Journal of Fluid Mech.*, Vol. 362, pp. 121~155.

Poinsot, T. J., Lele, S. K., 1992, "Boundary Conditions for Direct Simulations of Compressible Viscous Flows." *Journal of Computational Fluids*, 101, pp. 104~129.

Rayleigh, J. W. S., 1945, "The Theory of Sound," Vol. II, New York: Dover.

Richards, G. A.,1996, "Gas Turbine Combustion Instability," Technical Meeting of the Central State Section of the Combustion Institute, May 5~7, St. Louis MD.

Seo, S., 1999, "Combustion Instability Studies in Model Gas Turbine Combustors," Ph.D. Thesis, The Pennsylvania State University, University Park, PA.

Sung, H.-G., 1999, "Unsteady Flowfield in an Integral Rocket Ramjet Engine and Combustion Dynamics of a Gas turbine Swirl Stabilized Injector," Ph.D. Thesis, The Pennsylvania State University, University Park, PA.

Sirovich, L. E., 1987, "Turbulence and the Dynamics of Coherent Structures. Part I: Coherent Structures," Q. Appl. Math., XLV: 561~571.

Sirovich, L. E., Everson, R., 1992, "Management and Analysis of Large Scientific Datasets," *Int. Journal of Supercomputer Applications*, Vol. 6: 50.

Sirovich, L. E., Kirby, M., Winter, M., 1990, "An Eigenfunction Approach to Large Scale Transitional Structures in Jet Flows," *Phys. Fluids*, Vol. 2, pp. 127~135.

Torniainen, E. D., Hinz, A., Gouldin, F. C., 1997, "Tomographic Aanalysis of Unsteady, Reacting Flows," AIAA 97~0257.

Westbrook, C. K., Dryer, F.L., 1981, "Simplified Reaction Mechanisms for the Oxidation of Hydrocarbon," *Combustion Science and Technology*, Vol. 27, pp. 31~43.

Zhong, X., 1996, "Additive Semi-Implicit Runge-Kutta Method for Computing High-Speed Nonequilibrium Reactive Flows," *Journal of Computational Physics*, 128, pp. 19~31.